Digital nuclear morphometry correlates to BAP-1 expression, gene expression class and metastasis-free survival in uveal melanoma

Christina Herrspiegel[1,2], Thonnie Rose O. See[3], Pia R. Mendoza[4], Hans E. Grossniklaus[3], and Gustav Stålhammar*[1,2]

[1]St. Erik Eye Hospital, Stockholm, Sweden

[2]Department of Clinical Neuroscience, Karolinska Institutet, Stockholm, Sweden, and

[3]Departments of Ophthalmology and Pathology, Emory University School of Medicine, Atlanta, Georgia, USA.

[4]Department of Pathology and Laboratory Medicine, Emory University School of Medicine, Atlanta, Georgia, USA.

*Corresponding author

Gustav Stålhammar, M.D. Ph.D. FEBO

Oncology and Pathology service, St. Erik Eye Hospital

Department of Clinical Neuroscience, Karolinska Institutet

Polhemsgatan 50, 112 82

Stockholm, Sweden

Email: gustav.stalhammar@ki.se

Phone: +46 8 672 30 00

ABSTRACT

Cytologic features such as the shape and size of tumor cells can predict metastatic death in uveal melanoma, but suffer from poor reproducibility. In this study, we investigate the interobserver concordance of digital morphometry, and correlate the results with established prognostic markers. The average number of cells analyzed in each of 27 tumors, was 1957 (SD 349). Mean time consumption was less than 2.5 minutes per tumor. Identical morphometric classification was obtained for ≥ 85 % of tumors in all twelve evaluated morphometric variables (κ 0.70–0.93). The mean nucleus area, nucleus perimeter, nucleus max caliper and nucleus to cell area ratio were significantly greater in tumors with low nuclear BRCA associated protein-1 expression (nBAP-1) and gene expression class 2. Patients had significantly shorter metastasis-free survival if their tumors had low nBAP-1 expression (Log-Rank p=0.002), gene expression class 2 (Log-Rank p=0.004) or tumor cell nuclei with long max calipers (Log-Rank p=0.004) as defined in a training cohort and then tested in a validation cohort. We conclude that digital morphometry can be fast and highly reproducible, that for the first time, morphometry parameters can be objectively quantitated in thousands of cells at a time, and that variables describing the shape and size of the nuclei correlate to nBAP-1 expression, gene expression class and prognosis in uveal melanoma.

1. Introduction

Uveal melanoma is the most common primary intraocular malignancy in adults (Singh et al., 2014). Less than 5 % of patients have clinically detectable metastases at the time of diagnosis (Singh et al., 2014). At a later stage however, up to 45 % of patients will develop metastases even if the eye containing the tumor has been removed (Kujala et al., 2003). Once macrometastases develop, there is no effective treatment and median patient survival is only 4-12 months (Augsburger et al., 2009; Carvajal et al., 2016).

Several methods for prognostication are in clinical use. Tumor thickness, diameter, location in the eye and presence of distant metastases determine tumor stage (Arnljots et al., 2018; Kivelä et al., 2017). Loss of chromosome 3 has a high positive and negative predictive value for metastasis (Bornfeld et al., 1996). Commercial gene tests based on the expression of 12 classifier genes have been developed and show excellent prognostic utility in separation of class 1 tumors with low metastatic risk from class 2 tumors with high metastatic risk (Onken et al., 2012). Furthermore, we have previously shown the prognostic utility of manual (Szalai et al., 2018) and digital image analysis-based (Stålhammar et al., 2019) determination of the level of nBAP-1.

In 1931, Callender described six types of uveal melanoma based on cytologic features such as cell shape and the size of the nucleus (Callender, 1931). The original classification could accurately predict metastatic death, but suffered from substantial intra- and interobserver discordance (Coleman et al., 1996; Gamel et al., 1992). After several modifications, the morphological classification of uveal melanoma now rely on assessments of the proportion of epitheloid tumor cells (McLean et al., 1983;

Seddon et al., 1987). Examination of cytological features still require a high level of cytologic expertise and suffer from poor reproducibility (Gamel et al., 1992). Computer-assisted methods have therefore been proposed as a way of facilitating these assessments. In 1982, Gamel *et al*. found that 13 of 18 nuclear and nucleolar features correlated significantly with patient mortality when evaluated with a digitizer superimposed on microscopic images at a rate of 100 cells per hour (Gamel et al., 1982). Since then, computers have improved manyfold in terms of their computing power, cost and the number and scope of software applications and we can now analyze a dozen of variables or more in thousands of cells per minute on inexpensive off-the-shelf laptop computers (Stålhammar et al., 2016; Stålhammar et al., 2018).

Consequently, we see an opportunity to analyze cell morphometry features with digital image analysis and compare these to other prognostic factors including nBAP-1 expression in uveal melanoma patients from one American and one European referral center.

2. Methods

2.1. Patients and Samples

The study adhered to the tenets of the Declaration of Helsinki. Methods were carried out in accordance with the relevant guidelines and regulations. The protocol for collection of specimens and data from St. Erik Eye Hospital, Stockholm, Sweden was approved by the regional ethical review board in Stockholm, and the protocol for collection of specimens and data from Emory Eye Center, Atlanta, GA, USA by the Emory Institutional Review Board.

Patients were identified in the archives of the Oncology and Pathology service, St. Erik Eye Hospital and L.F. Montgomery Ophthalmic Pathology Laboratory, Emory Eye Center. Inclusion criteria were: 1) Enucleation performed before December 2017, 2) Histologically proven uveal melanoma, 3) paraffin block available, 4) gene expression classification available, 5) clinicopathological data available, including tumor thickness, diameter, location, T-category and cell type, 6) follow-up data available, 7) sufficient tissue for BAP-1 immunohistochemistry. Exclusion criteria were: 1) Prior history of plaque brachytherapy, proton beam irradiation and/or transpupillary thermotherapy, and 3) tumor fully necrotic or fully hemorrhagic. 27 patients met the criteria. Our follow-up data was confirmed and further extended in telephone interviews with patients or relatives. Informed consent was obtained from all participants.

In order to establish optimized morphometry thresholds for the distinction of metastatic versus non-metastatic disease we divided our 27 patients into one training and one validation cohort. When determining the relative size of the training and validation cohorts, we considered previous research indicating that the ratio should be inversely proportional to the square root of the number of free adjustable parameters (Guyon, 1997). As we only evaluated one morphometric variable at a time, we set the ratio to 1:1. 13 patients were randomized to the training cohort and 14 to the validation cohort.

2.2. Immunohistochemistry

The paraffin blocks were cut into 4 μm sections, pretreated in EDTA-buffer at pH 9.0 for 20 minutes and incubated with mouse monoclonal antibodies against BAP-1

(clone C-4, Santa Cruz Biotechnology, Dallas, Texas, USA) and a red chromogen, and finally counterstained with haematoxylin and rinsed with deionized water. The deparaffinization, pretreatment, primary staining, secondary staining and counterstaining steps were run in a Bond III automated IHC/ISH stainer (Leica, Wetzlar, Germany). Dilutions between 1:20 and 1:500 had been evaluated before selecting 1:40.

2.3. Digital image analysis

After sectioning and staining, all glass slides were digitally scanned to the .ndpi file format at ×400, using identical digital scanners at both institutions (Nano Zoomer 2.0 HT, Hamamatsu Photonics K.K., Hamamatsu, Japan). The digital image analysis (DIA) software used was the QuPath Bioimage analysis v. 0.2.0 m4 (Bankhead et al., 2017). The software was run on a standard off-the-shelf laptop computer (Apple Inc. Cupertino, CA).

For assessment of the level of nBAP-1 expression, one positive cell (red chromogen in nucleus) and one negative cell (haematoxylin but no red chromogen in nucleus) was calibrated in each digitally scanned tissue section. All other parameters were left at default in order to limit time consumption and maintain ease of use. Tumors were then screened under low magnification (40×) and the area exhibiting the most intense nBAP-1 staining selected for grading. Nuclear immunoreactivity was evaluated at 200×, in a circular 0.5 mm-diameter region of interest (corresponding to the field of view in a light microscope with a 400× objective) by automatic classification (positive cell detection). Based on previous publications, the nBAP-1 expression was classified as “high” if immunoreactivity was detected in >30 % of

tumor cells within the region of interest, and "low" if it was detected in ≤ 30 % of tumor cells (See et al., 2019; Stålhammar et al., 2019; Szalai et al., 2018).

A workflow for morphometric analysis was then created, including the following steps for each tumor: A) Identification of all cells within the region of interest, using the software's cell detection function with the following setttings: Background nucleus radius 8 µm, median filter radius 0 µm, sigma 1.5 µm, minimum nucleus area 7.5 μm^2, maximum nucleus area 200 μm^2, threshold 0.1, max background intensity 2 and cell expansion 5 µm. B) Measurement in each detected cell in each region of interest of the following 12 cell morphometric variables: 1) Nucleus area (μm^2). 2) Nucleus perimeter (µm). 3) Nucleus circularity. 4) Nucleus max caliper (µm). 5) Nucleus min caliper (µm). 6) Nucleus eccentricity. 7) Cell area (μm^2). 8) Cell perimeter (µm). 9) Cell circularity. 10) Cell max caliper. 11) Cell min caliper. 12) Nucleus to cell area ratio (figure 1).

Tumor areas with intense inflammation, heavy pigmentation, bleeding, necrosis or poor fixation were avoided. nBAP-1 classification and morphometric analysis was performed blinded to all other patient data including outcome. For measurement of interobserver concordance, two human observers performed the digital morphometry (morphometric variable above or below median value) and nBAP-1 classification (high or low) independently and blinded to patient outcomes.

2.4. Gene expression classification

Tumor tissue samples were obtained from freshly enucleated eyes by fine needle aspiration. The contents of the needle hub were transferred into one of two RNAse-free cryovials. Using the same needle, extraction buffer from the second cryovial was

aspirated and expelled into the first. This was then placed in a specimen bag, immediately frozen to -80° C and shipped on dry ice for gene expression classification based on 12 discriminating genes (*HTR2B, ECM1, RAB31, CDH1, FXR1, LTA4H, EIF1B, ID2, ROBO1, LMCD1, SATB1*, and *MTUS1*) and 3 control genes (*MRPS21*, *RBM23*, and *SAP130*) at a commercial laboratory (Castle Biosciences Inc. Friendswood, TX, USA). Expression levels of the gene products are used to categorize tumors as either class 1 with low metastatic risk, or class 2 with high metastatic risk (Onken et al., 2012).

2.5. Statistical methods

Differences with a $p<0.05$ were considered significant, all p-values being two-sided. The deviation of all clinicopathological variables from normal distribution was statistically significant, when evaluated by the Shapiro–Wilk test ($p<0.05$). For statistical tests of these variables, we therefore used the Mann-Whitney *U* test, which does not assume normally distributed data. The deviation of all morphometric variables from normal distribution was however not statistically significant ($p>0.05$), why we used Students T-tests for these. For comparisons of categorical variables, two-by-two tables and Fisher's exact test were used. For correlation to Cox Proportional Hazards for metastasis and Kaplan-Meier metastasis-free survival, patients were split into two groups based on 1) the median value of each morphometric variable, and 2) receiver operating characteristics (ROC) in the training cohort, with equal emphasis on sensitivity and specificity for the development of metastasis. The thresholds established in the training cohort were then tested in the validation cohort. In evaluation of interobserver concordance, the percentage of

identically classified cases and Cohen's kappa statistics (κ) were computed (Cohen, 1960). Metastasis-free follow-up was defined as the time in months from enucleation to the last occasion patients without metastases was seen or in contact alive. All statistical analyses were performed using IBM SPSS statistics version 25 (Armonk, NY, USA).

3. Results

3.1. Descriptive statistics

The mean age at enucleation of patients included in this study was 66 years (SD 15). Of 27 patients, 15 were men and 12 women. 25 tumors originated in the choroid and 2 in the ciliary body. The cell type was mixed in 18 patients, spindle in 5 and epitheloid in 4. Mean tumor thickness was 8.6 mm (SD 3.7) and mean diameter 15.8 mm (SD 4.8). 12 tumors were of gene expression class 2 and 15 of class 1a or 1b. 14 tumors had low nBAP-1 expression and 13 high. Mean metastasis-free follow-up time was 47 months (SD 76, Table 1).

The average number of cells analyzed in each tumor was 1957 (SD 349), which took an average of 74 seconds (SD 21) for nBAP-1 classification and 71 seconds (SD 17) for morphometric analysis, adding up to 145 seconds or nearly two-and-a-half minutes per tumor.

3.2. Interobserver concordance

Identical nBAP-1 classification was obtained for 25 of 27 tumors (93 %), yielding a Cohen's kappa statistic indicating almost perfect agreement (κ=0.85).

Identical morphometric classification (morphometric variable above/below median value) was obtained for ≥ 85 % of tumors in all 12 variables, yielding substantial or almost perfect agreement (κ 0.70–0.93, Table 2).

3.3. Morphometry versus nBAP-1 expression and gene expression class

The mean nucleus area, nucleus perimeter, nucleus max caliper and nucleus to cell area ratio were significantly greater in tumors with low nBAP-1 expression. Nucleus circularity, nucleus min caliper, nucleus eccentricity and cell area, cell perimeter, cell circularity, cell max and min caliper were however not significantly different (Table 3a).

Similarly, the mean nucleus area, nucleus perimeter, nucleus max caliper and nucleus to cell area ratio, but not the other morphometric variables, were significantly greater in tumors of gene expression class 2 (Table 3b).

3.4. Adjusted thresholds

The 4 morphometric variables that correlated to nBAP-1 and gene expression class were analyzed with ROC, with equal emphasis on sensitivity and specificity for the development of metastasis. Mean nucleus area achieved an area under the curve (AUC) of 0.67 (sensitivity 67 %, specificity 50 %, p=0.40) at threshold 27.5 μm^2; Mean nucleus perimeter achieved an area under the curve (AUC) of 0.73 (sensitivity 67 %, specificity 70 %, p=0.24) at threshold 21.5 μm; Mean nucleus max caliper achieved an area under the curve (AUC) of 0.80 (sensitivity 67 %, specificity 90 %, p=0.13) at threshold 8 μm; and mean nucleus to cell area ratio achieved an area under

the curve (AUC) of 0.60 (sensitivity 67 %, specificity 50 %, p=0.61) at threshold 0.28 (figure 2).

3.5. Regression analysis and survival

In univariate Cox proportional hazards analyses of nucleus area, nucleus perimeter, nucleus max caliper and nucleus to cell area ratio, none was an individual predictor of metastasis (Table 4).

In Kaplan-Meier analysis, patients had significantly shorter metastasis-free survival if their tumors had low nBAP-1 expression (Log-Rank p=0.002) or gene expression class 2 (Log-Rank p=0.004), but not if they had a mean nucleus area, nucleus perimeter, nucleus max caliper and nucleus to cell area ratio greater than the median (Log-Rank p=0.20–0.83). When using the thresholds established in the training cohort, mean nucleus max caliper > 8 μm was associated with metastasis-free survival (Log-Rank p=0.05), whereas the other ROC-adjusted variables did not separate groups with significant survival differences (Log-rank p=0.18–0.95, figure 3).

4. Discussion

In this study, we have shown that digital image analysis of uveal melanoma cell morphometry can be fast and highly reproducible, and that variables describing the shape and size of the nuclei correlate to nBAP-1 expression as well as gene expression class. Patients with tumors that had large nuclei, as defined by their max caliper, had significantly worse prognosis. On the other hand, no variable describing the shape and size of the entire tumor cell correlated to the established prognostic

253 factors, indicating that for prognosis, the morphological characteristics of tumor
254 nuclei are more important.

255 The prognostic importance of cell morphology is by no means a novel
256 discovery. However, reproducibility, time consumption and level of expertise
257 required to make reliable assessments of morphometry have limited its utility.
258 Modern user-friendly digital image analysis techniques offer an attractive solution to
259 these problems, and for the first time we can now objectively quantitate morphometry
260 parameters in thousands of cells at a time.

261 In turn, changes to the size and shape of tumor cells are but a consequence of
262 changes in the genotype. As found by Onken *et al*. the helix-loop-helix inhibitor *ID2*
263 suppress the epithelial phenotype associated with an enlarged nucleus (Onken et al.,
264 2006). Loss of *ID2* up-regulates the epithelial adhesion molecule E-cadherin, which in
265 turn promotes the anchorage-independent cell growth required for metastasis.
266 Consequently, we regard the morphometric characteristics investigated here as
267 biomarkers of the state of the genotype.

268 Limitations of this study include a small sample size. Inclusion of a larger
269 number of patients may have revealed additional significant differences. This was
270 however prevented, primarily by the lack of tumors in our archives for which gene
271 expression classification was available. Far-reaching conclusions from our survival
272 analysis are thereby precluded. Substantial investments in digital scanning capacity is
273 required before the method presented here can be used. The time consumption
274 specified will most likely be longer for users without general experience in the
275 operation of home computers, and does not include preanalytical operations such as
276 digital scanning and loading and unloading of glass slides. Last, our sample is not

representative of all patients with uveal melanoma. We have only investigated the feasibility of digital morphometry in enucleated specimens without previous plaque brachytherapy. A large proportion of patients with uveal melanoma undergo primary plaque brachytherapy or proton beam radiotherapy, and may never require enucleation. It remains unclear if the digital morphometry characteristics of small uveal melanomas is different from the relatively large tumors investigated here. Accordingly, we encourage future studies to confirm these results in larger cohorts that includes smaller tumors .

Funding

This work was supported in part by Cancerfonden, Karolinska Institutet (Karolinska Institutets stiftelsemedel för ögonforskning) and Stockholm County Council (Stockholms läns landsting).

References

Arnljots, T.S., Al-Sharbaty, Z., Lardner, E., All-Eriksson, C., Seregard, S., Stålhammar, G., 2018. Tumour thickness, diameter, area or volume? The prognostic significance of conventional versus digital image analysis-based size estimation methods in uveal melanoma. Acta Ophthalmol 96, 510-518.

Augsburger, J.J., Corrêa, Z.M., Shaikh, A.H., 2009. Effectiveness of Treatments for Metastatic Uveal Melanoma. American Journal of Ophthalmology 148, 119-127.

Bankhead, P., Loughrey, M., Fernández, J., Dombrowski, Y., McArt, D., Dunne, P., McQuaid, S., Gray, R., Murray, L., Coleman, H., James, J., Salto-Tellez, M., Hamilton, P., 2017. QuPath: Open source software for digital pathology image analysis. Sci Rep 7, 16878-16878.

Bornfeld, N., Prescher, G., Becher, R., Hirche, H., Jöckel, K.H., Horsthemke, B., 1996. Prognostic implications of monosomy 3 in uveal melanoma. The Lancet 347, 1222-1225.

Callender, G., 1931. Malignant Melanotic tumors of the eye. A study of histologic types in 111 cases. Trans. Am. Acad. Ophthalmol. Otolaryngol. 36, 131-142.

Carvajal, R.D., Schwartz, G.K., Tezel, T., Marr, B., Francis, J.H., Nathan, P.D., 2016. Metastatic disease from uveal melanoma: treatment options and future prospects. British Journal of Ophthalmology.

Cohen, J., 1960. A Coefficient of Agreement for Nominal Scales. Educational and Psychological Measurement 20, 37-46.

Coleman, K., Baak, J.P.A., van Diest, P.J., Mullaney, J., 1996. Prognostic Value of Morphometric Features and the Callender Classification in Uveal Melanomas. Ophthalmology 103, 1634-1641.

Gamel, J.W., McCurdy, J.B., McLean, I.W., 1992. A comparison of prognostic covariates for uveal melanoma. Investigative ophthalmology & visual science 33, 1919.

Gamel, J.W., McLean, I.W., Greenberg, R.A., Zimmerman, L.E., Lichtenstein, S.J., 1982. Computerized histologic assessment of malignant potential: A method for determining the prognosis of uveal melanomas. Human Pathology 13, 893-897.

Guyon, I., 1997. A scaling law for the validation-set training-set size ratio. At&t Bell Laboratories, Berkeley California, pp. 1-11.

Kivelä, T., Simpson, E.R., Grossniklaus, H.E., Jager, M.J., Singh, A.D., Caminal, J.M., Pavlick, A.C., Kujala, E., Coupland, S.E., Finger, P.T., 2017. Uveal Melanoma, AJCC Cancer Staging Manual, 8 ed. Springer, Chicago, pp. 805-817.

Kujala, E., Mäkitie, T., Kivelä, T., 2003. Very long-term prognosis of patients with malignant uveal melanoma. Invest Ophthalmol Vis Sci 44, 4651-4659.

McLean, I., Foster, W., Zimmerman, L., Gamel, J., 1983. Modifications of Callender's classification of uveal melanoma at the Armed Forces Institute of Pathology. Am J Ophthalmol 96, 502-509.

Onken, M.D., Ehlers, J.P., Worley, L.A., Makita, J., Yokota, Y., Harbour, J.W., 2006. Functional gene expression analysis uncovers phenotypic switch in aggressive uveal melanomas. Cancer research 66, 4602.

Onken, M.D., Worley, L.A., Char, D.H., Augsburger, J.J., Correa, Z.M., Nudleman, E., Aaberg, T.M., Altaweel, M.M., Bardenstein, D.S., Finger, P.T., Gallie, B.L., Harocopos, G.J., Hovland, P.G., McGowan, H.D., Milman, T., Mruthyunjaya, P., Simpson, E.R., Smith, M.E., Wilson, D.J., Wirostko, W.J., Harbour, J.W., 2012. Collaborative Ocular Oncology Group report number 1: prospective validation of a multi-gene prognostic assay in uveal melanoma. Ophthalmology 119, 1596-1603.

Seddon, J.M., Polivogianis, L., Hsieh, C.-C., Albert, D.M., Gamel, J.W., Gragoudas, E.S., 1987. Death From Uveal Melanoma: Number of Epithelioid Cells and Inverse SD of Nucleolar Area as Prognostic Factors. Archives of Ophthalmology 105, 801-806.

See, T.R.O., Stålhammar, G., Phillips, S.S., Grossniklaus, H.E., 2019. BAP1 Immunoreactivity Correlates with Gene Expression Class in Uveal Melanoma. Ocular Oncology and Pathology, 1-9.

Shields, C.L., Furuta, M., Thangappan, A., Nagori, S., Mashayekhi, A., Lally, D.R., Kelly, C.C., Rudich, D.S., Nagori, A.V., Wakade, O.A., Mehta, S., Forte, L., Long, A., Dellacava, E.F., Kaplan, B., Shields, J.A., 2009. Metastasis of Uveal Melanoma Millimeter-by-Millimeter in 8033 Consecutive Eyes. Archives of Ophthalmology 127, 989-998.

Singh, N., Bergman, L., Seregard, S., Singh, A.D., 2014. Epidemiologic Aspects, in: Damato, B., Singh, A.D. (Eds.), Clinical Ophthalmic oncology: Uveal tumors, 2 ed. Springer, Berlin, Heidelberg, pp. 75-87.

Stålhammar, G., Fuentes Martinez, N., Lippert, M., Tobin, N.P., Mølholm, I., Kis, L., Rosin, G., Rantalainen, M., Pedersen, L., Bergh, J., Grunkin, M., Hartman, J., 2016. Digital image analysis outperforms manual biomarker assessment in breast cancer. Modern pathology : an official journal of the United States and Canadian Academy of Pathology, Inc 29, 318.

Stålhammar, G., Robertson, S., Wedlund, L., Lippert, M., Rantalainen, M., Bergh, J., Hartman, J., 2018. Digital image analysis of Ki67 in hot spots is superior to both manual Ki67 and mitotic counts in breast cancer. Histopathology 72, 974-989.

Stålhammar, G., See, T.R.O., Phillips, S., Seregard, S., Grossniklaus, H.E., 2019. Digital Image Analysis of BAP-1 Accurately Predicts Uveal Melanoma Metastasis. Translational vision science & technology 8, 11.

Szalai, E., Wells, J.R., Ward, L., Grossniklaus, H.E., 2018. Uveal Melanoma Nuclear BRCA1-Associated Protein-1 Immunoreactivity Is an Indicator of Metastasis. Ophthalmology 125, 203-209.

Legends

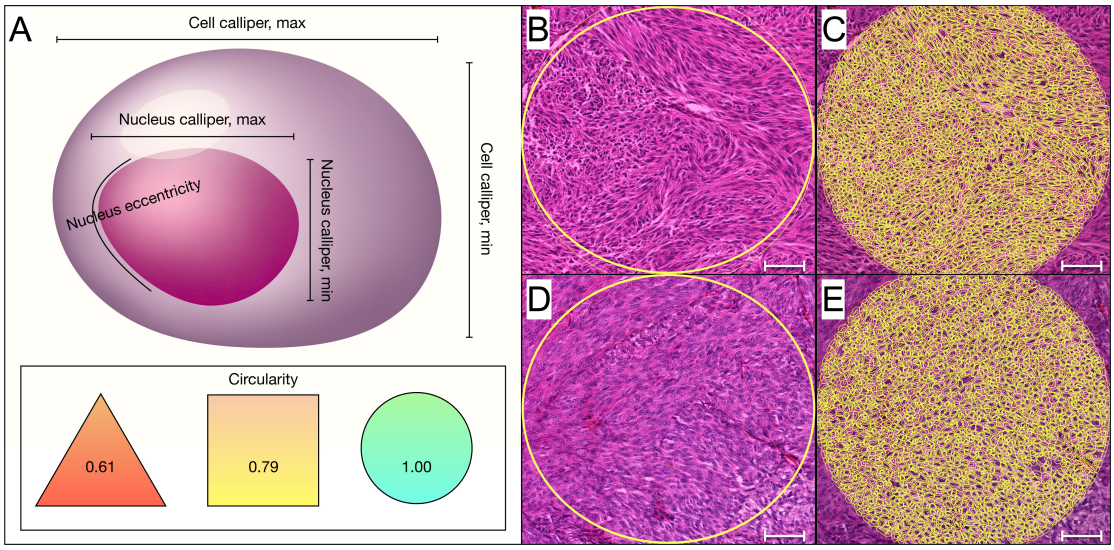

Figure 1. Illustration of cell morphometric measurements. A) Calipers denotes the largest and smallest diameters of the nucleus and cell. Nucleus eccentricity is a measure of how much the nucleus deviates from a spherical shape, presented as a number between 0.00 and 1.00. A completely spherical nucleus have an eccentricity of 0.00, a nucleus with the shape of an elliptical 3D solid would have an eccentricity

of 0.5, whereas a 3D conical distribution would have a value of 1.00. Circularity compares the perimeter of a shape to the area it contains, and is calculated by four times π times the area divided by the perimeter squared. The circularity of a circle is 1.00, and less for less circular objects. B) A circular 0.5 mm-diameter region of interest (corresponding to the field of view in a light microscope with a 400× objective) was defined in each tumor. Within this region of interest, each cell was analyzed for nBAP-1 expression and 12 morphometric variables describing the size and shape of cells and nuclei. C) The morphometric variables have been automatically identified within the region of interest shown in B. D and E) In another tumor, cells have slightly larger, more rounded nuclei with prominent nucleoli, corresponding to what would be known as epitheloid cells. Cell illustration by iStock.com/Vitalii Dumma, East Ukraine Volodymyr Dahl National University Scale bars: 100 µm..

***n* =**	27
Mean age at diagnosis, years (SD)	66 (15)
Sex, n (%)	
Female	15 (56)
Male	12 (44)
Primary tumor location, n (%)	
Choroid	25 (93)
Ciliary body	2 (7)
Iris	0 (0)
Cell type, n (%)	
Spindle	5 (19)
Epitheloid	4 (15)
Mixed	18 (67)
Mean tumor thickness, mm (SD)	8.6 (3.7)

Mean tumor diameter, mm (SD)	15.8 (4.8)
Previous brachytherapy or TTT, n (%)	
No	27 (100)
Yes	0 (0)
AJCC T-category, n (%)	
1	0 (0)
2	7 (26)
3	14 (52)
4	6 (22)
Gene expression class, n (%)	
1a	9 (33)
1b	6 (22)
2	12 (44)
DIA nBAP-1 classification, n (%)	
High	13 (48)
Low	14 (52)
Follow-up months, mean (SD)[§]	47 (76)

393 Table 1. Characteristics of patients and tumors included in this study. SD, standard

394 deviation. TTT, Transpupillary thermotherapy.

395

	Interobserver concordance (%)	**Cohen's κ**
Nucleus area	85	0.70
Nucleus perimeter	85	0.70
Nucleus circularity	96	0.93
Nucleus caliper, max	85	0.70
Nucleus caliper, min	89	0.78
Nucleus eccentricity	96	0.93
Cell area	85	0.70
Cell perimeter	85	0.70
Cell circularity	93	0.85
Cell caliper, max	85	0.70

Cell caliper, min	85	0.70
Nucleus to cell area ratio	96	0.93

Table 2. Interobserver concordance and Cohen's kappa statistics in classification of each morphometric variable as above or below the median value.

	nBAP-1 high (n=13)	**nBAP-1 low (n=14)**	***P***
Nucleus area, μm^2 (SD)	24.31 (4.38)	28.34 (3.40)	0.013
Nucleus perimeter, µm (SD)	19.61 (1.78)	21.37 (1.28)	0.0066
Nucleus circularity	0.76 (0.04)	0.75 (0.04)	0.41
Nucleus caliper, max µm (SD)	7.52 (0.65)	8.21 (0.58)	0.0074
Nucleus caliper, min µm (SD)	4.43 (0.59)	4.67 (0.36)	0.20
Nucleus eccentricity (SD)	0.76 (0.03)	0.77 (0.04)	0.52
Cell area, μm^2 (SD)	88.50 (15.10)	94.58 (12.42)	0.26
Cell perimeter, µm (SD)	37.05 (3.26)	38.33 (2.53)	0.26
Cell circularity	0.77 (0.01)	0.77 (0.01)	0.70
Cell caliper, µm (SD)	13.62 (1.22)	14.09 (0.97)	0.27
Cell caliper, µm (SD)	9.00 (0.79)	9.29 (0.59)	0.30
Nucleus to cell area ratio	0.28 (0.03)	0.30 (0.02)	0.031

Table 3a.

Average values and Students T-tests of cell morphometric variables in tumors of high versus low nBAP-1 expression. SD, standard deviation.

	Gene expression class 1a or 1b (n=15)	**Gene expression class 2 (n=12)**	***P***
Nucleus area, μm^2 (SD)	24.89 (4.40)	28.28 (3.59)	0.041
Nucleus perimeter, µm (SD)	19.84 (1.76)	21.37 (1.39)	0.0022
Nucleus circularity	0.76 (0.04)	0.75 (0.04)	0.42

Nucleus caliper, max µm (SD)	7.59 (0.63)	8.23 (0.63)	0.016
Nucleus caliper, min µm (SD)	4.48 (0.57)	4.65 (0.37)	0.39
Nucleus eccentricity (SD)	0.76 (0.03)	0.77 (0.04)	0.33
Cell area, μm^2 (SD)	89.90 (14.59)	93.83 (13.16)	0.48
Cell perimeter, µm (SD)	37.34 (3.13)	38.18 (2.70)	0.47
Cell circularity	0.77 (0.01)	0.77 (0.01)	0.64
Cell caliper, max µm (SD)	13.71 (1.15)	14.06 (1.05)	0.42
Cell caliper, min µm (SD)	9.23 (0.61)	9.23 (0.61)	0.62
Nucleus to cell area ratio	0.28 (0.03)	0.30 (0.02)	0.024

403 Table 3b.

404 Average values and Students T-tests of cell morphometric variables in tumors of gene

405 expression class 1a or 1b versus 2. SD, standard deviation.

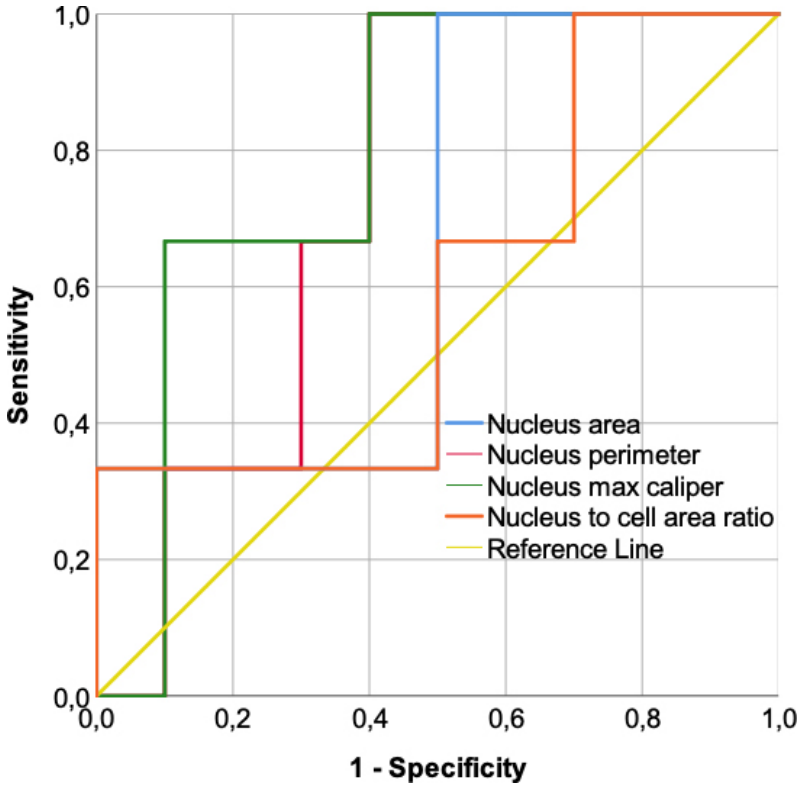

406

407 Figure 2.

Receiver operating characteristics (ROC) of the mean nucleus area, nucleus perimeter, nucleus max caliper and nucleus to cell area ratio in the training cohort (*n*=13), with equal emphasis on sensitivity and specificity for the development of metastasis. Mean nucleus area (blue line) achieved an area under the curve (AUC) of 0.67 (sensitivity 67 %, specificity 50 %, p=0.40) at threshold 27.5 μm^2; Mean nucleus perimeter (pink line) achieved an area under the curve (AUC) of 0.73 (sensitivity 67 %, specificity 70 %, p=0.24) at threshold 21.5 μm; Mean nucleus max caliper (green line) achieved an area under the curve (AUC) of 0.80 (sensitivity 67 %, specificity 90 %, p=0.13) at threshold 8 μm; and mean nucleus to cell area ratio (orange line) achieved an area under the curve (AUC) of 0.60 (sensitivity 67 %, specificity 50 %, p=0.61) at threshold 0.28.

	Regression coefficient, β (SE)	**Wald statistic**	***P***	**Hazard coefficient, Exp(b) (95 % CI)**
Univariate Cox proportional hazards				
Nucleus area ≥ median	0.2 (0.7)	0.05	0.83	1.17 (0.3–4.8)
Nucleus perimeter ≥ median	0.9 (0.7)	1.5	0.22	2.5 (0.6–10.4)
Nucleus caliper, max ≥ median	0.9 (0.7)	1.5	0.22	2.5 (0.6–10.4)
Nucleus to cell area ratio ≥ median	0.4 (0.7)	0.4	0.52	1.6 (0.4–5.9)

Table 4.

Cox Proportional Hazards analysis of the association between metastasis-free survival and cell morphometric variables. No method was individually associated with shortened metastasis-free survival.

SE, standard error.

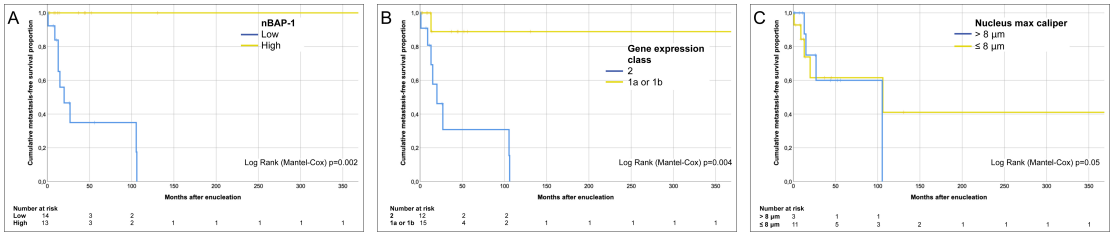

Figure 3.

Kaplan-Meier curves, cumulative metastasis-free survival. A) Patients with tumors with high nBAP-1 expression (yellow) versus low (blue), as defined by digital image analysis using a mean of <30 % stained tumor nuclei as cutoff (Log-Rank p=0.002). B) Patients with tumors of gene expression class 1a or 1b (yellow) versus 2 (blue, Log-Rank p=0.004). C) Patients in the validation cohort (*n*=14) with mean nucleus max caliper ≤ 8 µm (yellow) versus > 8 µm (blue), which was the threshold established in the training cohort (Log-Rank p=0.05).

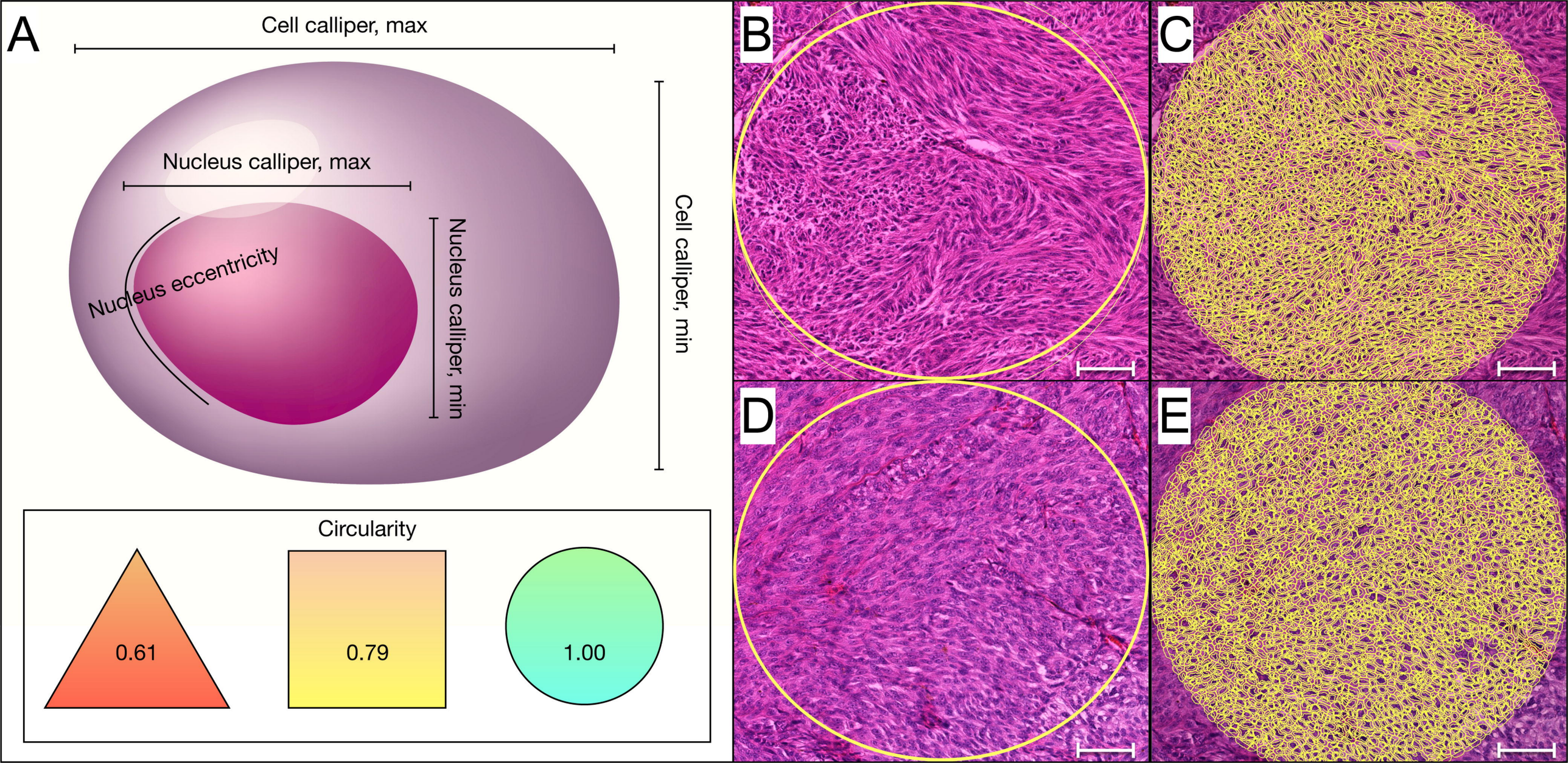
A
Cell calliper, max
Nucleus calliper, max
Nucleus eccentricity
Nucleus calliper, min
Cell calliper, min
Circularity
0.61
0.79
1.00
B
C
D
E

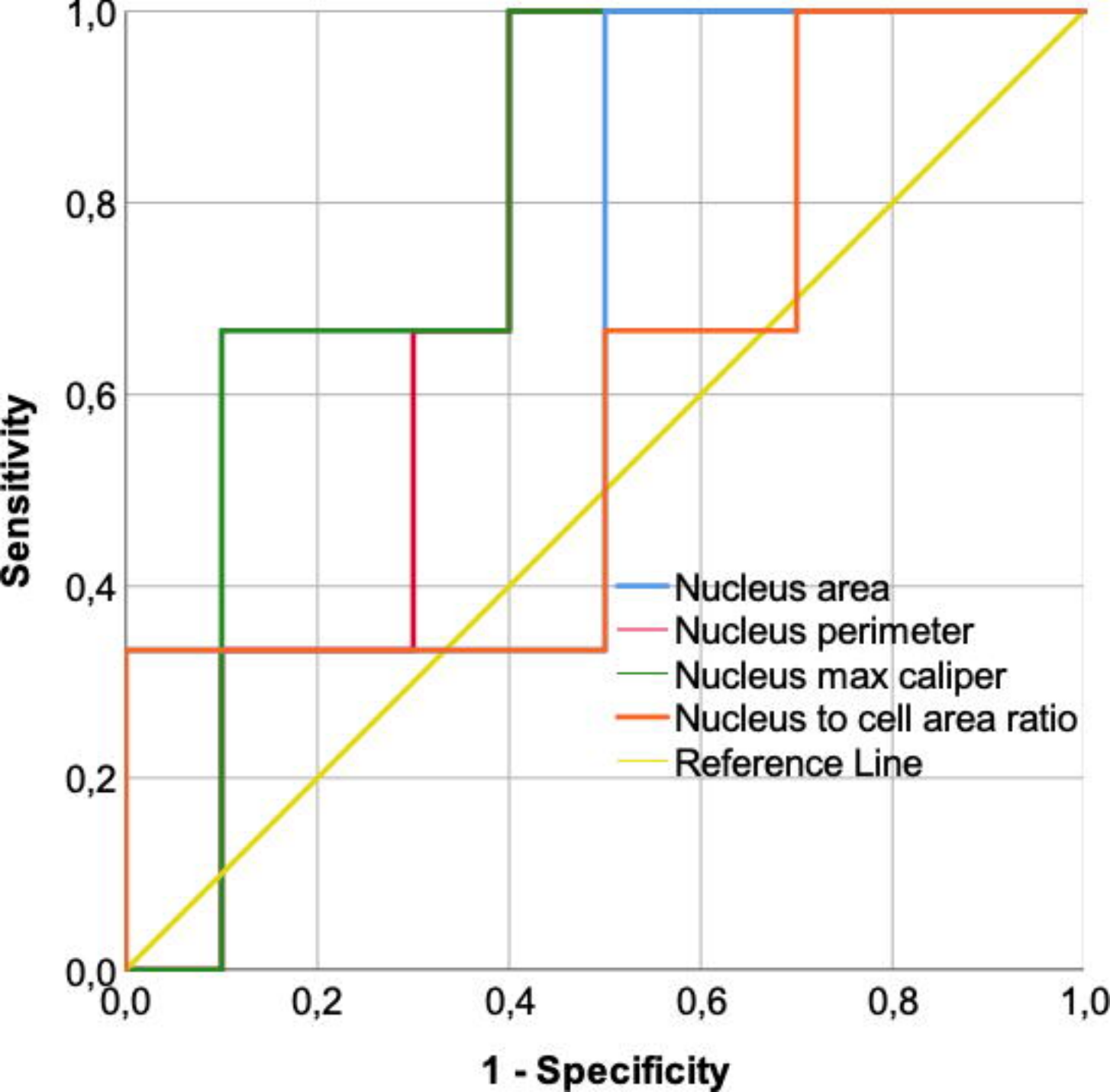
Sensitivity
1,0
0,8
0,6
0,4
0,2
0,0
0,0
0,2
0,4
0,6
0,8
1,0
1 - Specificity
Nucleus area
Nucleus perimeter
Nucleus max caliper
Nucleus to cell area ratio
Reference Line

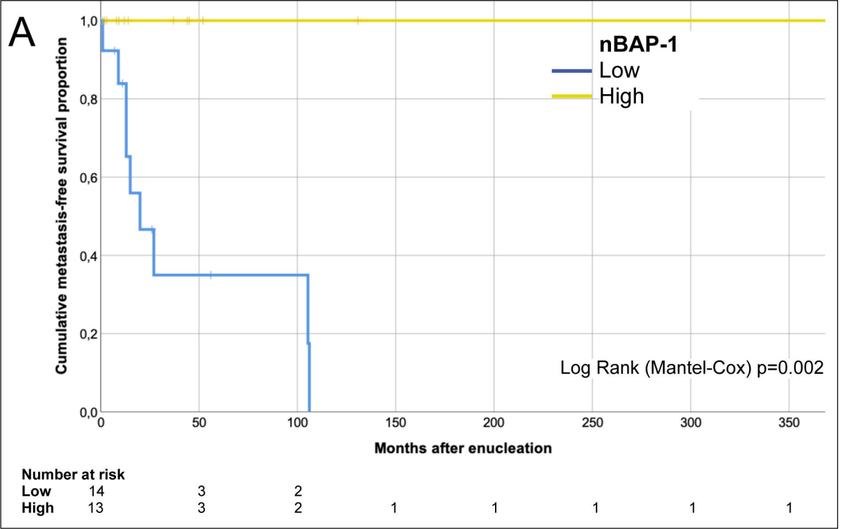
A
nBAP-1
Low
High
Cumulative metastasis-free survival proportion
1,0
0,8
0,6
0,4
0,2
0,0
0
50
100
150
200
250
300
350
Months after enucleation
Log Rank (Mantel-Cox) p=0.002
Number at risk
Low 14 3 2
High 13 3 2 1 1 1 1 1

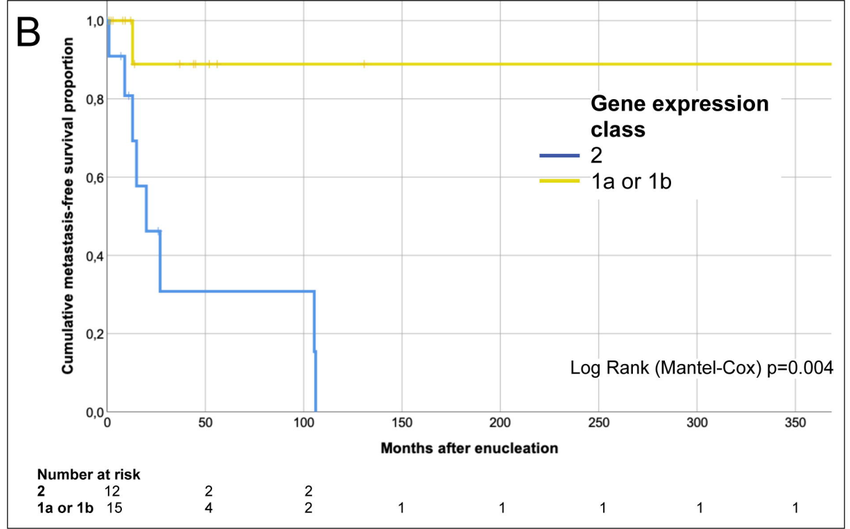
B
Gene expression class
2
1a or 1b
Cumulative metastasis-free survival proportion
1,0
0,8
0,6
0,4
0,2
0,0
0
50
100
150
200
250
300
350
Months after enucleation
Log Rank (Mantel-Cox) p=0.004
Number at risk
2 12 2 2
1a or 1b 15 4 2 1 1 1 1 1

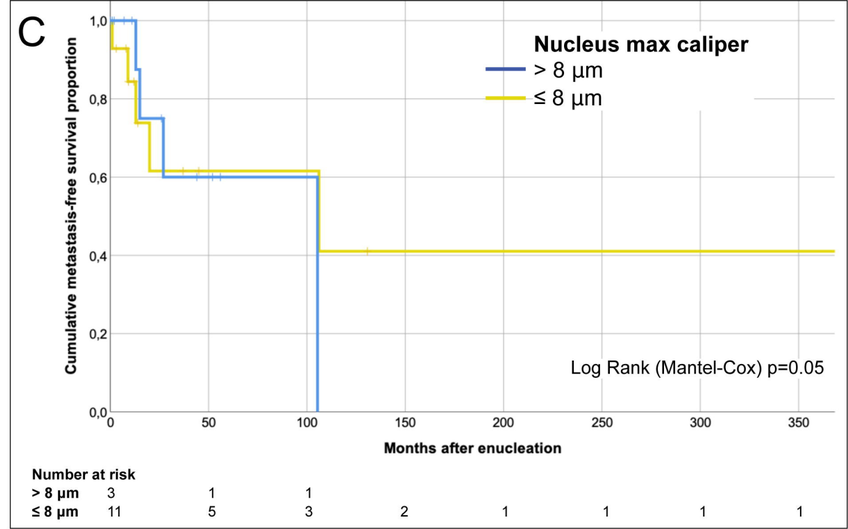
C
Nucleus max caliper
> 8 µm
≤ 8 µm
Cumulative metastasis-free survival proportion
1,0
0,8
0,6
0,4
0,2
0,0
0
50
100
150
200
250
300
350
Months after enucleation
Log Rank (Mantel-Cox) p=0.05
Number at risk
> 8 µm 3 1 1
≤ 8 µm 11 5 3 2 1 1 1 1